Solid State Electronics xxx (xxxx) xxx–xxx

Contents lists available at ScienceDirect

Solid State Electronics

journal homepage: www.elsevier.com/locate/sse

Effects of structure and oxygen flow rate on the photo-response of amorphous IGZO-based photodetector devices

Jun Tae Jang[1], Daehyun Ko[1], Sungju Choi, Hara Kang, Jae-Young Kim, Hye Ri Yu, Geumho Ahn, Haesun Jung, Jihyun Rhee, Heesung Lee, Sung-Jin Choi, Dong Myong Kim, Dae Hwan Kim*

School of Electrical Engineering, Kookmin University, 77 Jeongneung-ro, Seongbuk-gu, Seoul 02707, Republic of Korea

ARTICLE INFO

Keywords:
Amorphous-IGZO (a-IGZO) photodetector
Structure dependence
Oxygen flow rate (OFR) dependence
Persistent-photoconductivity (PPC)
Sub-gap density-of-states (DOS)
Oxygen vacancy (V_O) ionization
Charge trapping
Threshold voltage (V_T) decomposition

ABSTRACT

In this study, we investigated how the structure and oxygen flow rate (OFR) during the sputter-deposition affects the photo-responses of amorphous indium-gallium-zinc-oxide (a-IGZO)-based photodetector devices. As the result of comparing three types of device structures with one another, which are a global Schottky diode, local Schottky diode, and thin-film transistor (TFT), the IGZO TFT with the gate pulse technique suppressing the persistent photoconductivity (PPC) is the most promising photodetector in terms of a high photo-sensitivity and uniform sensing characteristic. In order to analyze the IGZO TFT-based photodetectors more quantitatively, the time-evolution of sub-gap density-of-states (DOS) was directly observed under photo-illumination and consecutively during the PPC-compensating period with applying the gate pulse. It shows that the increased ionized oxygen vacancy (V_O^{2+}) defects under photo-illumination was fully recovered by the positive gate pulse and even overcompensated by additional electron trapping. Based on experimentally extracted sub-gap DOS, the origin on PPC was successfully decomposed into the hole trapping and the V_O ionization. Although the V_O ionization is enhanced in lower OFR (O-poor) device, the PPC becomes more severe in high OFR (O-rich) device because the hole trapping dominates the PPC in IGZO TFT under photo-illumination rather than the V_O ionization and more abundant holes are trapped into gate insulator and/or interface in O-rich TFTs. Similarly, the electron trapping during the PPC-compensating period with applying the positive gate pulse becomes more prominent in O-rich TFTs. It is attributed to more hole/electron traps in the gate insulator and/or interface, which is associated with oxygen interstitials, or originates from the ion bombardment-related lower quality gate oxide in O-rich devices.

1. Introduction

At the advent of the Internet-of-Things (IoT) age, flexible and stretchable application-compatible technologies that can integrate the circuits with sensors using a single material are becoming increasingly necessary especially in wearable and healthcare fields [1–8]. Amorphous indium-gallium-zinc-oxide (a-IGZO) is particularly promising for such a material as it has high mobility, is transparent in the visible-light range, can be uniform over large areas, is processed at low temperatures, and is promising for the use of temperature and/or photo sensor devices [3,5]. Indeed, a-IGZO has been studied by a large number of research groups for it to be used successfully in flexible and stretchable applications [3–8].

One of the applications of a-IGZO that is being studied is its use as a photodetector that can detect various photon energies (E_{ph}) and optical powers (P_{op}) over an infrared to ultraviolet range of light; a-IGZO is of particular interest owing to its large bandgap ($E_g > 3$ eV) and amorphous channel material that has a sub-gap ($E_V < E_{ph} < E_C$) density-of-states (DOS) related to the randomness of the metal cations, *i.e.*, In, Ga, and Zn as well as induced by the details of fabrication process [9,10]. However, the IGZO-based photodetectors have inherent limitation in terms of their photo-sensitivity and reproducible photo-response, because they have the persistent photoconductivity (PPC) which means the phenomenon that electrically conductive characteristics after photo-illumination remains even under light-off conditions [11–14]. Accordingly, research into IGZO-based photodetectors has been devoted either to the proposal of the PPC-free measurement technique in phototransistor configuration, e.g., the gate pulse-combined PPC suppression in IGZO thin-film transistors (TFTs) [11], or to the control of oxygen vacancy (V_O)-related defects in IGZO TFTs because the PPC is well known to be associated with the photo-response of V_O-related defects [12,13]. However, a qualitative analysis of the change of sub-

* Corresponding author.
E-mail address: drlife@kookmin.ac.kr (D.H. Kim).
[1] J.T. Jang and D. Ko contributed equally to this work.

http://dx.doi.org/10.1016/j.sse.2017.10.028

gap DOS has barely been researched in terms of a dynamic photo-response of IGZO phototransistor, although both controlling V_O density and applying the pulse of gate bias would affect the sub-gap DOS significantly [11]. Furthermore, from the viewpoint of photodetector structure, the IGZO photodiode configuration has been rarely compared with the IGZO phototransistor configuration even though the Schottky diode has been generally formed between the IGZO and many kinds of metal electrodes [15].

In this study, we investigated the structural effect on the photo-responses of a-IGZO-based photodetectors by comparing the photodiode configuration with the phototransistor configuration. To begin with, we analyzed the optical response by measuring the current-voltage (I-V) and transient characteristics in structure-dependent devices, where the IGZO devices used were bottom-gate TFTs, global Schottky (GS) and local Schottky (LS) diodes. Furthermore, in order to analyze a dynamic photo-response of IGZO TFT more quantitatively, the change of sub-gap DOS was traced before and after the photo-illumination as well as was characterized with varying the V_O density, which is modulated by varying the oxygen flow rate (OFR) during the sputter-deposition of IGZO film as the active layer of TFT. In addition, we used a pulse-measurement technique to remove PPC from the photodetector and then qualitatively analyzed the difference of sub-gap DOS between just after the photo-illumination and after applying the gate bias pulse. The OFR-dependent PPC and recovery enhanced by the gate pulse were explained with the experimental observation of the dynamic change of sub-gap DOS.

2. Influence of the structure on the photo-response in a-IGZO-based photodetector devices

In order to investigate how the structure of the a-IGZO-based photodetector devices influenced their optical response, three different types of a-IGZO-based devices were fabricated, i.e., bottom-gate TFT, GS and LS diodes as shown in Fig. 1(a)–(c). The procedure of fabrication process is as follows. A thermally grown 50-nm-thick SiO_2 layer on a heavily-doped p^+-Si substrate was used as the gate insulator and gate electrode for the a-IGZO TFT, while an e-beam-evaporated 60-nm-thick Au layer was used as the bottom electrode in the a-IGZO GS and LS diodes. An a-IGZO layer was sputter-deposited at a working pressure of 5 mTorr and at an RF power of 150 W. The Ar:O_2 gas mixture during the sputtering was different for the TFTs and the Schottky diodes (3:0.1 sccm as compared with 3:0.5 sccm). The a-IGZO layers of the TFT and LS diode were deposited with an active shadow mask, but the GS diode was deposited without a shadow mask. An 80-nm-thick Ti layer was used for the source and drain electrodes in the TFT; the layer was deposited using an e-beam evaporator by using an electrode shadow mask and subsequently annealed in air for 1 h at 250 °C. On the other hand, a 60-nm-thick Au top electrode was deposited using an e-beam evaporator with a top electrode shadow mask in the GS and LS diodes.

Fig. 1(d)–(f) shows the I-V characteristics of the three different a-IGZO-based devices; these characteristics were measured using an Agilent 4156C precision semiconductor parameter analyzer at a room temperature dark ambient. To measure the transfer characteristics of the a-IGZO TFT, the gate-source voltage (V_{GS}) was swept forward from −10 to 15 V and in reverse from 15 to −10 V at a fixed drain-source voltage (V_{DS}) of 0.1 V, respectively, as depicted in Fig. 1(d). In this figure, the electrical characteristics of the a-IGZO TFT are the threshold voltage (V_T) = 0.02 V at $I_{DS} = 10^{-9}$ A, subthreshold slope (SS) = 0.11 V/dec at $I_{DS} = 10^{-11}$ to 10^{-9} A, and field-effect mobility at linear region ($\mu_{FE,Lin}$) = 10.75 $cm^2 V^{-1} s^{-1}$ at V_{GS} = 15 V. In the case of the I-V characteristics of the GS and LS diodes, the top electrode voltage (V_{TE}) was swept forward from 0 to 2.5 V and in reverse from 0 to −2.5 V, while the bottom electrode was grounded as shown in Fig. 1(e) and (f). Furthermore, the current of the GS diode was higher than that of the LS diode due to an additional fringing current path around the Au top electrode in the GS diode.

In order to investigate the transient photo-response characteristics, either the drain-to-source current (I_{DS}) in TFT or the top electrode current (I_{TE}) in diode was defined as the read-out current (I_{READ}), and the I_{READ} was characterized over time. Either the V_{GS} with V_{DS} = 0.1 V

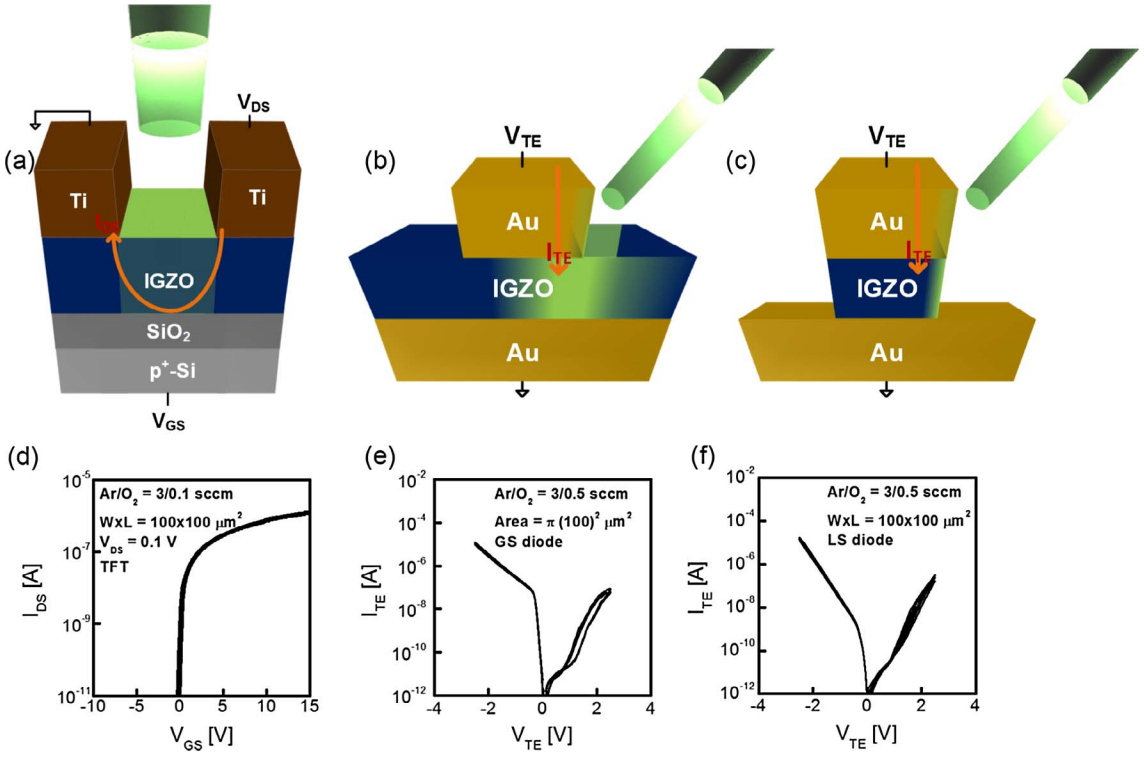

Fig. 1. Schematic illustration of the a-IGZO-based devices of (a) the TFT, (b) the GS diode, and (c) the LS diode. The I-V characteristics of the (d) TFT, (e) GS diode, and (f) LS diode are also shown.

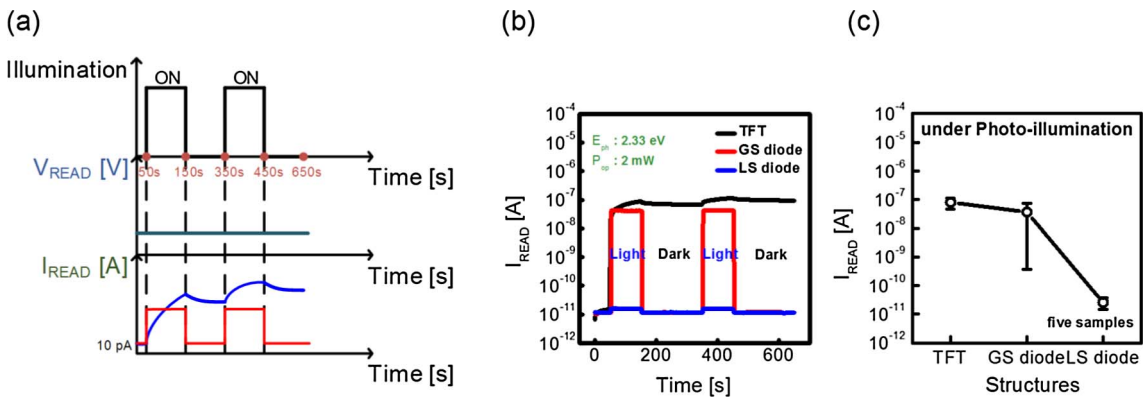

Fig. 2. (a) Measurement sequences for the three different types of a-IGZO-based devices under bias-illumination conditions. (b) The measured photo-response current during a repetitive light/dark sequence. (c) The photocurrent uniformity of five samples of each of the three structures.

in TFT or the V_{TE} in diode was also defined as the read-out voltage (V_{READ}). Procedure of measuring the transient photo-response was illustrated in Fig. 2(a). Photo-illumination was applied twice with a light pulse of E_{ph} = 2.33 eV and P_{op} = 2 mW by using the optical fiber as seen in Fig. 1(a)–(c). The V_{READ} was set for I_{READ} to be 10 pA before applying a photo-illumination and was maintained throughout a whole measurement.

Measured I_{READ} over time is given in Fig. 2(b), and the I_{READ}'s under photo-illumination are summarized for five samples as shown in Fig. 2(c). Fig. 2(b) suggests that the photo-sensitivity becomes higher in the order of LS diode, GS diode, and TFT. However, the PPC is observed only in TFT case. Fig. 2(c) shows that the uniformity of photo-response is very poor especially in GS diode case. Regardless of the PPC phenomenon, the optical response of the a-IGZO TFT was influenced across the entire channel, and the light response of the diodes was affected in the local space. Notably, the GS diode had a higher current than the LS diode regardless of the dark/photo conditions used, because the additional current path affected electron movement. However, since the diodes were locally illuminated, the uniformity of I_{READ} was extremely sensitive to the direction, angle, and area of the incident light, which was not the case in the TFT. In Fig. 2(b) and (c), it is found that the a-IGZO TFT is the most desirable among three types of photodetectors only if the PPC can be suppressed because it shows a high photo-sensitivity as well as a good uniformity, i.e., the immunity to the direction and/or angle of incident light.

Here, it is worthwhile to note that the removal method of the PPC characteristic from an a-IGZO TFT is already known [11–14]. Therefore, we chose the TFT as a promising photodetector configuration and analyzed the optical responses and sub-gap DOS of the a-IGZO TFTs more in detail by changing the V_O density via modulating OFR during the sputter-deposition of IGZO.

3. Oxygen flow rate-dependent electrical characteristics in a-IGZO TFTs

In order to analyze the photo-response of a-IGZO TFT more quantitatively, first of all, the high-performance inverted staggered bottom-gate a-IGZO TFTs with an etch-stop layer were fabricated as shown in Fig. 3(a). The fabrication procedure for the a-IGZO TFTs was as follows; to begin with, molybdenum (Mo) was sputter deposited so that it could be used as the metal gate on a glass substrate. A 50-nm-thick SiN_x layer and a 400-nm-thick SiO_x layer were then deposited via plasma-enhanced chemical vapor deposition (PECVD) at 370 °C to form the gate insulator (the equivalent oxide thickness was 258 nm). A 50-nm-thick IGZO layer was then deposited via DC magnetron sputtering at a gas flow rate of Ar:O_2 = 35:21 sccm (O—Poor), 35:42 sccm (O-Medium), and 35:63 sccm (O-Rich) at a total pressure of 5 mTorr. The sputtering power was controlled so as to remain at 2 kW at room temperature. Either the OFR or the oxygen partial pressure during the sputter-deposition of IGZO has been widely used for controlling the V_O density [16–20]. The etch stopper SiO_x layer was deposited via PECVD at 150 °C and patterned by wet etching. In order to form the source/drain (S/D) electrode, Mo was sputtered at room temperature and patterned by dry etching. Finally, the fabricated devices were thermally annealed at 250 °C for 1 h. The channel width (W) and length (L) of the devices were 50 and 50 μm, respectively.

Fig. 3(b) and (c) shows the transfer characteristics in the a-IGZO TFT with the OFR at V_{DS} = 0.1 V, and its electrical parameters with the OFR are depicted in Fig. 3(d)–(g). The hysteresis voltage (V_{Hys}) was extracted from difference of V_Ts at $I_{DS} = 10^{-9}$ A of forwardly and reversely swept transfer characteristics. As the OFR increases, the V_T, SS, and V_{Hys} are higher, while the $\mu_{FE,Lin}$ becomes lower.

In addition, we extracted the sub-gap DOS by using the optical response of the C-V characteristics, i.e., monochromatic photonic C-V (MPCV) technique [21], as described in Fig. 4(a). The measurement conditions of the C-V characteristics were as follows: E_{ph} = 2.82 eV, P_{op} = 4 mW, and the AC signal frequency = 50 kHz. The sub-gap DOS of the a-IGZO TFTs with OFR was extracted as described in Fig. 4(b) and (c), and the sub-gap DOS parameters are summarized in Table 1 where the $g_A(E)$ and $g_D(E)$ are the acceptor-like and donor-like DOS, respectively. While the $g_A(E)$ consists of g_{TA}, g_{DA}, and g_{O-O}, the $g_D(E)$ is composed of g_{TD}, g_{Vo}, and g_{Vo2+}. We found that the one Gaussian function in E_V + 0.15 eV (g_{O-O}) and two exponential functions (g_{TA} and g_{DA}) near the conduction band minimum (E_C) were higher for higher OFR, while the one Gaussian function in E_V + 1.1 eV (g_{Vo}) and the one Gaussian function in E_C-0.05 eV (g_{Vo2+}) were higher for lower OFR, and the one exponential function near E_V (g_{TD}) was nearly constant, as shown in Fig. 4(b) and (c). First of all, the higher sub-gap DOS observed at the E_V + 1.1 eV and E_C − 0.05 eV levels with the lower OFR strongly correlated with the neutral and ionized oxygen vacancy defects (V_O and V_O^{2+}) which are known to have a donor-like nature [22–24]. Furthermore, the higher sub-gap DOSs with the higher OFR obtained at the E_V + 0.15 eV level were the valence band tail states due to amorphous random network and were corroborated with metastable defects (ppπ*), which are known to have an acceptor-like nature [25]. These defects are generally understood to be the origin of the instability under bias-illumination associated with the hole-mediated peroxide formation [25]. Furthermore, the existence of the two exponential functions near E_C can be explained by the ion bombardment during the DC sputtering, which is attributed to influence the quality of the gate oxide and oxide/channel interface, as has been previously reported [26]. Sub-gap DOSs near E_C are consistent with the electrical characteristics in a-IGZO TFTs with the OFR as shown in Fig. 3(d)–(g). As the OFR increases, the V_T increases with the decrease of shallow donor defects V_O^{2+} while the SS increases and the $\mu_{FE,Lin}$ decreases with the increase of g_{TA} and g_{DA}.

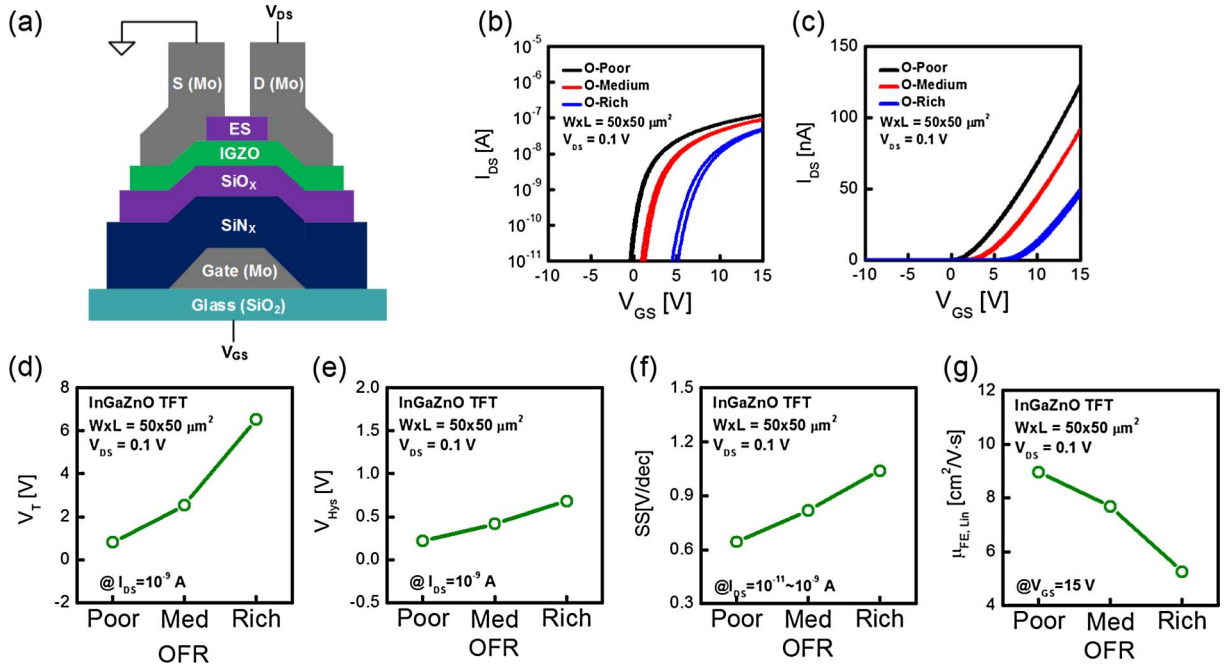

Fig. 3. (a) Schematic illustration of the inverted staggered bottom-gate a-IGZO TFT that had an etch-stop layer. The initial transfer characteristics of the a-IGZO TFTs with the OFR at (b), (c) V_{DS} = 0.1 V are shown. From the transfer characteristics, we were able to extract the (d) V_T, (e) V_{Hys}, (f) SS, and (g) $\mu_{FE,\ Lin}$.

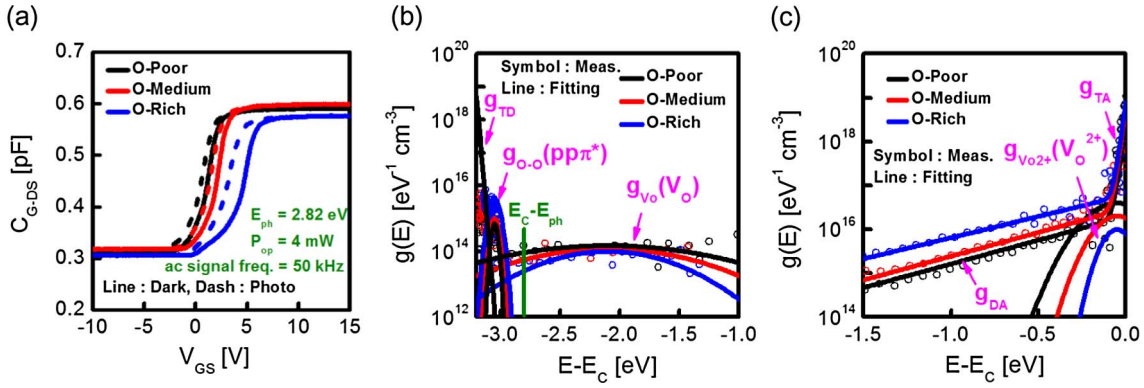

Fig. 4. (a) Measured C-V characteristics under dark and sub-bandgap photonic states with OFR. The extracted energy distribution of the sub-gap DOS through the MPCVS of (b) $g_D(E)$ and (c) $g_A(E)$.

Table 1
Extracted sub-gap DOS parameters with OFR by MPCVS.

	O-Poor	O-Medium	O-Rich
$g_A(E) = g_{TA}(E) + g_{DA}(E) + g_{o-o}(E) = N_{TA} \times \exp\left(\frac{E-E_C}{kT_{TA}}\right) + N_{DA} \times \exp\left(\frac{E-E_C}{kT_{DA}}\right) + N_{o-o} \times \exp\left(-\left(\frac{(E_V-E)+E_{o-o}}{kT_{o-o}}\right)^2\right)$			
N_{TA}/kT_{TA} [eV^{-1} cm^{-3}/eV]	$3 \times 10^{18}/0.015$	$6 \times 10^{18}/0.015$	$8 \times 10^{18}/0.015$
N_{DA}/kT_{DA} [eV^{-1} cm^{-3}/eV]	$2 \times 10^{16}/0.4$	$3 \times 10^{16}/0.4$	$6 \times 10^{16}/0.45$
$N_{o-o}/E_{o-o}/kT_{o-o}$ [eV^{-1} cm^{-3}/eV/eV]	$0.7 \times 10^{15}/0.15/0.03$	$1 \times 10^{15}/0.15/0.04$	$4 \times 10^{15}/0.15/0.05$
$g_D(E) = g_{TD}(E) + g_{Vo}(E) + g_{Vo2+}(E) = N_{TD} \times \exp\left(\frac{E_V-E}{kT_{TD}}\right) + N_{Vo} \times \exp\left(-\left(\frac{(E_V-E)+E_{Vo}}{kT_{Vo}}\right)^2\right) + N_{Vo2+} \times \exp\left(-\left(\frac{(E-E_C)+E_{Vo2+}}{kT_{Vo2+}}\right)^2\right)$			
N_{TD}/kT_{TD} [eV^{-1} cm^{-3}/eV]	$5 \times 10^{18}/0.01$	$5 \times 10^{18}/0.01$	$5 \times 10^{18}/0.01$
$N_{Vo}/E_{Vo}/kT_{Vo}$ [eV^{-1} cm^{-3}/eV/eV]	$1.5 \times 10^{14}/1.1/1$	$1.2 \times 10^{14}/1.1/0.8$	$1 \times 10^{14}/1.1/0.6$
$N_{Vo2+}/E_{Vo2+}/kT_{Vo2+}$ [eV^{-1} cm^{-3}/eV/eV]	$4 \times 10^{16}/0.05/0.2$	$2 \times 10^{16}/0.05/0.2$	$1 \times 10^{16}/0.05/0.2$

4. Effect of the oxygen flow rate on photo-response in a-IGZO TFTs

Fig. 5(a) shows the measurement sequence under light-illumination and the gate pulse in the a-IGZO TFTs, which was similar to the experimental procedure depicted in Fig. 2(a). In addition, the gate pulse was applied with V_{GS} = 20 V during 0.1 s to eliminate the PPC effect after photo-illumination. As shown in Fig. 5(b), we observed higher optical sensitivity and larger PPC characteristics in the a-IGZO TFTs that had higher OFR. Noticeably, this observation is different from the previous work [16], where the IGZO TFT with higher density of V_Os became less stable under the negative bias illumination stress (NBIS). This issue will be discussed later.

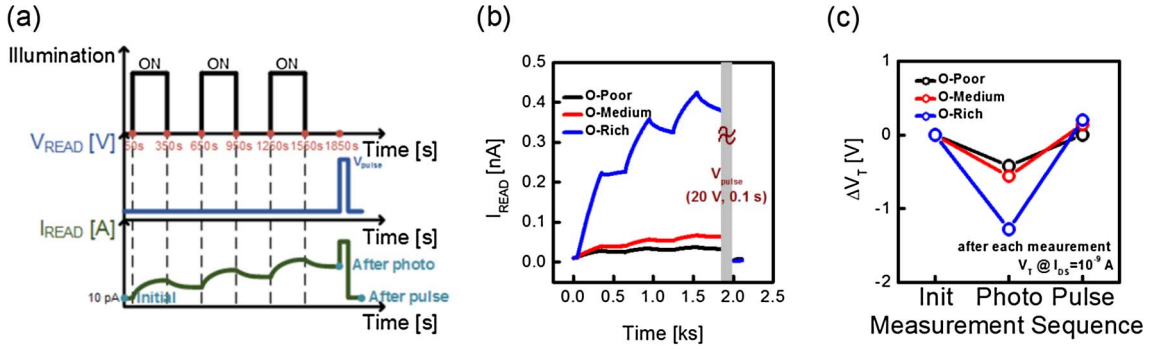

Fig. 5. (a) Measurement sequence of the a-IGZO TFTs with OFR under bias-illumination and gate pulse conditions. (b) Measured read current during the repetitive light/dark sequence and gate pulse. (c) Extracted delta V_T with the measurement sequence and OFR.

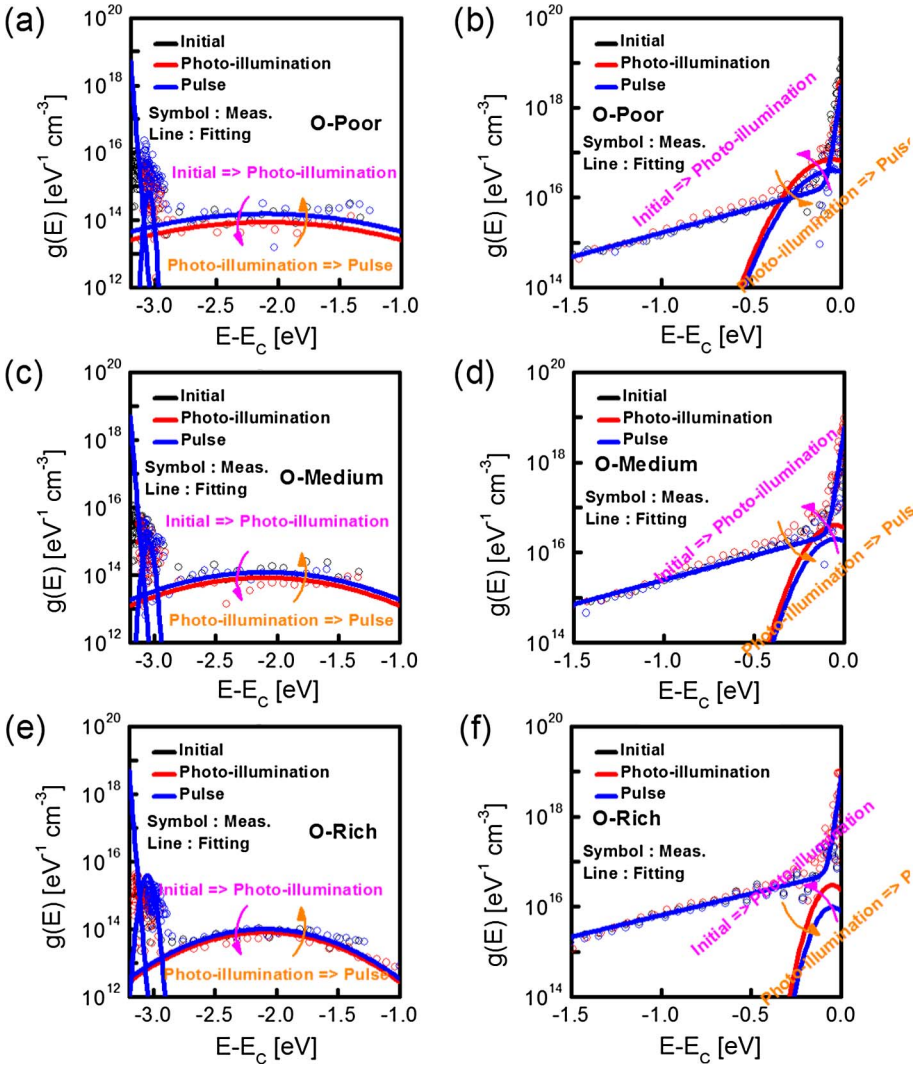

Fig. 6. Extracted energy distribution of the sub-gap DOSs through the MPCVS. g(E) near (a), (c), (e) E_V and (b), (d), (f) E_C in the a-IGZO TFTs with the (a), (b) O-Poor, (c), (d) O-Medium, and (e), (f) O-Rich.

The V_T shift (ΔV_T) after consecutive gate pulse measurement as well as that after three times photo-illumination is shown in Fig. 5(c). Consistently with Fig. 5(b), the magnitude of negative ΔV_T after photo-illumination increases in O-rich TFTs. In Fig. 5(c), the ΔV_T becomes close to zero again after applying the gate pulse irrespective of OFR, which suggests the gate pulse condition used is well optimized for suppressing the PPC [11].

The PPC or NBIS instability mechanisms under bias-illumination conditions in a-IGZO TFTs are already known: (1) positive charge (hole) trapping into gate oxide or in the interface layer [28–30]; (2) V_O ionization model [22–24], *i.e.*, $V_O \rightarrow V_O^{2+} + 2e^-$; (3) hole-mediated peroxide formation model [25], *i.e.*, $(O\text{-}O)^{2-} + 2h^+ \rightarrow O_2^{2-} + 2e^- + 2h^+$. The ambient effect can be excluded owing to the passivation in the IGZO channel [31]. Therefore, we analyzed and decomposed the effects of the photo-illumination instability and the pulse measurement by considering these three instability mechanisms, so that we could investigate the origin of the reliability degradation in IGZO TFT-based photodetectors.

For the characterization before and after photo-illumination and pulse measurement with the OFR, we extracted the sub-gap DOS via the

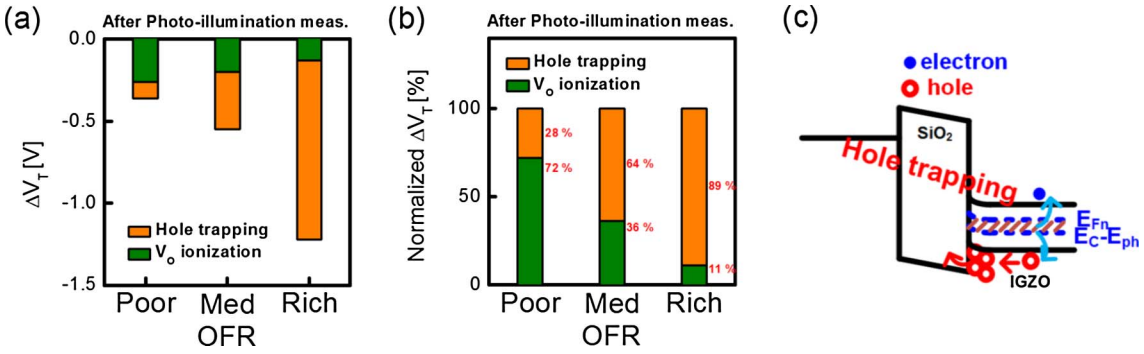

Fig. 7. (a) Decomposed ΔV_T and (b) normalized decomposed ΔV_T for a portion of the hole trapping and V_O ionization models with OFR after the photo-illumination measurement. (c) Schematic illustration of the hole trapping of a-IGZO TFTs after the photo-illumination measurement.

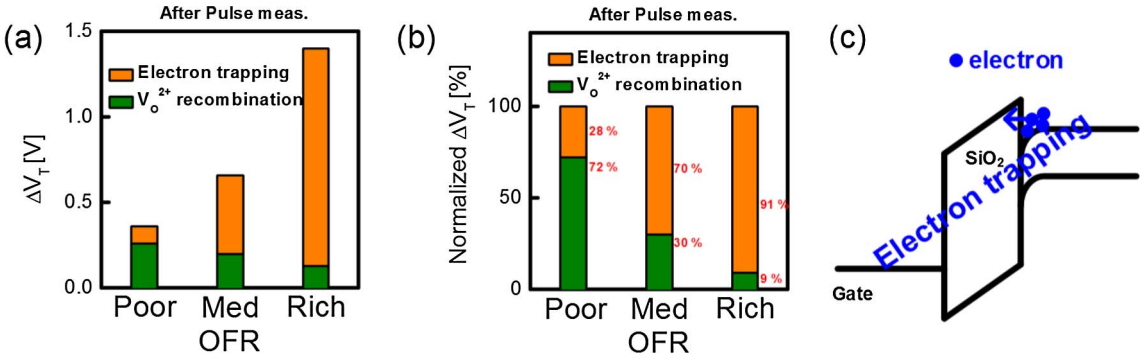

Fig. 8. (a) Decomposed ΔV_T and (b) normalized decomposed ΔV_T for a portion of the electron trapping and V_O^{2+} recombination models with OFR after the pulse measurement. (c) Schematic illustration of the electron trapping of a-IGZO TFTs after the pulse measurement.

MPCVS in the a-IGZO TFTs with the OFR during the measurement sequence, as shown in Fig. 6. Thus, we experimentally confirmed that g_{Vo} and g_{VO2+} decreased and increased, respectively, under photo-illumination regardless of the OFR [Fig. 6], which is consistent with the V_O ionization model as the origin on PPC. The peroxide formation can be also excluded from the PPC origin because the $E_C - E_{ph}$ level does not be overlapped with $g_{O\text{-}O}$ as seen in Fig. 4(b). We also observed that the g_{Vo2+} increased under photo-illumination was fully recovered after pulse measurement irrespective of the OFR [Fig. 6]. In order to qualitatively decompose the ΔV_T during the photo-illumination and/or the gate pulsed recovery into the hole trapping-induced and the V_O ionization-induced component, the following equation for the ΔV_T component due to the change of g_{Vo2+} can be used:

$$\Delta V_{T,Vo2+} = qT_{act}\frac{\int_E \Delta g_{Vo2+}(E)dE}{C_{ox}}, \quad (1)$$

where $\Delta V_{T,Vo2+}$ is the V_O ionization-induced ΔV_T component, C_{ox} is the gate oxide capacitance per unit area, and T_{act} is the active layer thickness. Then, the hole trapping-induced ΔV_T component can be calculated from a total $\Delta V_T - \Delta V_{T,Vo2+}$ because the peroxide formation can be excluded as abovementioned. By using $\Delta V_{T,Vo2+}$, total ΔV_T and the normalized ΔV_T decomposed as a portion of the charge trapping and V_O ionization models are summarized, as described in Fig. 7. We confirmed that the O-rich IGZO TFT shows larger ΔV_T, less V_O^{2+} creation, and more pronounced hole trapping. Here, it should be noted that the OFR-dependence of $\Delta V_{T,Vo2+}$ is consistent with the previous study [27]. However, in our case, the OFR-dependence of total ΔV_T due to PPC is opposite to [16] because the hole trapping dominates the PPC-induced ΔV_T rather than the V_O ionization. The reason why more abundant holes are trapped into gate insulator bulk or interface as the OFR increases can be explained as follows. The first is that the quality of gate oxide becomes degraded with the increase of OFR because the ion bombardment becomes harsher during the sputter-deposition of IGZO on the gate insulator [26], which can be also the origin on higher g_{TA} and g_{DA} with higher OFR. The second is that as the IGZO oxygen content increases, a larger number of oxygen atoms can diffuse into the SiO_2 gate insulator owing to the strong Si–O affinity. Increased oxygen interstitials can generate hole and/or electron traps in the gate insulator [32], which is consistent with relatively poor GI quality, i.e., larger hysteresis in O-rich devices as shown in Fig. 3(e).

In order to remove the PPC effect, we used the gate pulse measurement technique, as depicted in Fig. 5(a). ΔV_T and the normalized ΔV_T are summarized in Fig. 8. After the pulse measurement, V_T shifted positively rather than remaining in its initial state, as shown in Fig. 5(c). Although V_O^{2+} was fully recovered, as shown in Fig. 6, the additional charge trapping could affect V_T after a strong pulse. Therefore, we found that the instability under light-illumination can result from the additional electron trapping effect if the device is subject to a strong ion bombardment effect, such as the O-Rich a-IGZO TFTs with poor oxide and interface quality, despite the presence of the V_O ionization mechanism.

5. Conclusion

We investigated the effects of structure and OFR on the photo-response of a-IGZO-based photodetector devices. It was found that the IGZO TFT with the gate pulse technique suppressing the PPC is a promising photodetector in terms of a high photo-sensitivity and an uniform sensing characteristic rather than the IGZO GS and/or LS diode. The time-evolution of sub-gap DOS in IGZO TFTs was directly observed during photo-illumination and the recovery period applying the gate pulse. It suggests that the increased g_{Vo2+} under photo-illumination was fully recovered by the positive gate pulse.

Based on experimentally extracted sub-gap DOS, the origin on PPC was successfully decomposed into the hole trapping and the V_O ionization. Although the V_O ionization happens more actively in lower OFR (O-poor) device, the PPC becomes more severe in high OFR (O-rich) device because the hole trapping dominates the PPC in IGZO TFT under

photo-illumination rather than the V_O ionization and the hole trapping is more accelerated in O-rich TFTs. Similarly, the electron trapping during the PPC compensation period applying the positive gate pulse becomes more prominent in O-rich TFTs. It can be attributed either to more abundant hole/electron traps in the gate insulator and/or interface, which is associated with oxygen interstitials, or to the ion bombardment-related lower quality gate oxide in O-rich devices.

Our results suggest that the joint-optimization of gate insulator and a-IGZO film is indispensable for the IGZO-based photodetector applications in the wearable IoT era.

Acknowledgement

This work was supported by the National Research Foundation of Korea (NRF) Grant funded by the Korean Government (MSIP) under Grant 2016R1A5A1012966.

References

[1] Gao W, Nyein Hnin YY, Shahpar Z, Tai LC, Wu E, Bariya M, et al. Wearable sweat biosensors. IEEE Int Electron Dev Meet 2016:161–4.
[2] Alharbi A, Nasri B, Wu T, Shahrjerdi D. Advanced integrated sensor and layer transfer technologies for wearable bioelectronics. IEEE Int Electron Dev Meet 2016:157–60.
[3] Takei K. High performance, flexible CMOS circuits and sensors toward wearable healthcare applications. IEEE Int Electron Dev Meet 2016:143–6.
[4] Cantarella G, Munzenrieder N, Petti L, Vogt C, Buthe L, Salvatore GA, et al. Flexible In-Ga-Zn-O thin-film transistors on elastomeric substrate bent to 2.3% strain. IEEE Electron Dev Lett 2015;36(8):781–3.
[5] Knobelspies S, Daus A, Cantarella G, Petti L, Münzenrieder N, Tröster G, et al. Flexible a-IGZO phototransistor for instantaneous and cumulative UV-exposure monitoring for skin health. Adv Electron Mater 2016;2(10):1600273.
[6] Yoon J, Jeong Y, Kim H, Yoo S, Jung HS, Kim Y, et al. Robust and stretchable indium gallium zinc oxide-based electronic textiles formed by cilia-assisted transfer printing. Nat Commun 2016;7:11477.
[7] Heremans P, Papadopoulos N, De Jamblinne, De Meux A, Nag M, Steudel M, et al. Flexible metal-oxide thin film transistor circuits for RFID and health patches. IEEE Int Electron Dev Meet 2016:151–4.
[8] Li X, Hasan M, Jeon J, Jang J. Stretchable oxide TFTs for wearable electronics. SID Symp Dig Tech Pap 2017:42–5.
[9] Noh HK, Chang KJ, Ryu B, Lee WJ. Electronic structure of oxygen-vacancy defects in amorphous In-Ga-Zn-O semiconductors. Phys Rev B 2011;84(11):115205.
[10] Noh HK, Park JS, Chang KJ. Effect of hydrogen incorporation on the negative bias illumination stress instability in amorphous In-Ga-Zn-O thin-film-transistors. J Appl Phys 2013;113(6):063712.
[11] Lee S, Nathan A, Jeon S, Robertson J. Oxygen defect-induced metastability in oxide semiconductors probed by gate pulse spectroscopy. Sci Rep 2015;5:14902.
[12] Lee S, Nathan A, Ye Y, Guo Y, Robertson J. Localized tail states and electron mobility in amorphous ZnON thin film transistors. Sci Rep 2015;5:13467.
[13] Ghaffarzadeh K, Nathan A, Robertson J, Kim S, Jeon S, Kim C, et al. Persistent photoconductivity in Hf-In-Zn-O thin film transistors. Appl Phys Lett 2010;97(14):143510.
[14] Kim HS, Jeon SH, Park JS, Kim TS, Son KS, Seon JB, et al. Anion control as a strategy to achieve high-mobility and high-stability oxide thin-film transistors. Sci Rep 2013;3:1459.
[15] Trinh TT, Nguyen VD, Nguyen HH, Raja J, Jang J, Jang K, et al. Operation mechanism of Schottky barrier nonvolatile memory with high conductivity InGaZnO active layer. Appl Phys Lett 2012;100(14):143502.
[16] Jang JT, Park J, Ahn BD, Kim DM, Choi SJ, Kim HS, et al. Study on the photoresponse of amorphous In-Ga-Zn-O and zinc oxynitride semiconductor devices by the extraction of sub-gap-state distribution and device simulation. ACS Appl Mater Interf. 2015;7(28):15570–7.
[17] Kim JS, Kim YM, Jeong KS, Yun HJ, Yang SD, Kim SH, et al. A light-induced threshold voltage instability based on a negative-U center in a-IGZO TFTs with different oxygen flow rates. Trans Electr Electron Mater 2014;15(6):315–9.
[18] Ling L, Tao X, Zhongxiao S, Chunliang L, Fei M. Effect of sputtering pressure on surface roughness, oxygen vacancy and electrical properties of a-IGZO thin films. Rare Met Mater Eng 2016;45(8):1992–6.
[19] Sahoo AK, Wu GM. Effects of argon flow rate on electrical properties of amorphous indium gallium zinc oxide thin-film transistors. Thin Solid Films 2016;605:129–35.
[20] Wu CH, Yang FC, Chen WC, Chang CL. Influence of oxygen/argon reaction gas ratio on optical and electrical characteristics of amorphous IGZO thin films coated by HiPIMS process. Surf Coat Technol 2016;303:209–14.
[21] Bae H, Choi H, Jun S, Jo C, Kim YH, Hwang JS, et al. Single-scan monochromatic photonic capacitance-voltage technique for extraction of subgap DOS over the bandgap in amorphous semiconductor TFTs. IEEE Electron Dev Lett 2013;34(12):1524–6.
[22] Ryu B, Noh HK, Choi EA, Chang KJ. O-vacancy as the origin of negative bias illumination stress. Appl Phys Lett 2010;97(2):022108.
[23] Um JG, Mativenga M, Jang J. Mechanism of positive bias stress-assisted recovery in amorphous-indium-gallium-zinc-oxide thin-film transistors from negative bias under illumination stress. Appl Phys Lett 2013;103(3):033501.
[24] Oh H, Yoon SM, Ryu MK, Hwang CS, Yang S, Park SHK. Photon-accelerated negative bias instability involving subgap states creation in amorphous In–Ga–Zn–O thin film transistor. Appl Phys Lett 2010;97(18):183502.
[25] Nahm HH, Kim YS, Kim DH. Instability of amorphous oxide semiconductors via carrier-mediated structural transition between disorder and peroxide state. Phys Status Solidi Basic Res 2012;249(6):1277–81.
[26] Kim S, Jeon YW, Kim Y, Kong D, Jung HK, Bae MK, et al. Impact of oxygen flow rate on the instability under positive bias stresses in DC-sputtered amorphous InGaZnO thin-film transistors. IEEE Electron Dev Lett 2012;33(1):62–4.
[27] Kim DH, Kim W, Kim Y, Hur I, Bae M, Kong D, et al. Physical model and simulation platform for high-level instability-aware design of amorphous oxide semiconductor thin-film transistors. SID Symp Dig Tech Pap 2012:10–4.
[28] Chen TC, Chang TC, Hsieh TY, Lu WS, Jian FY, Tsai CT, et al. Investigating the degradation behavior caused by charge trapping effect under DC and AC gate-bias stress for InGaZnO thin film transistor. Appl Phys Lett 2011;99(2):022104.
[29] Cho IT, Lee JM, Lee JH, Kwon HI. Charge trapping and detrapping characteristics in amorphous InGaZnO TFTs under static and dynamic stresses. Semicond Sci Technol 2008;24(1):015013.
[30] Chen TC, Chang TC, Tsai CT, Hsieh TY, Chen SC, Lin CS, et al. Behaviors of InGaZnO thin film transistor under illuminated positive gate-bias stress. Appl Phys Lett 2010;97(11):112104.
[31] Yang S, Cho DH, Ryu MK, Park SHK, Hwang CS, Jang J, et al. Improvement in the photon-induced bias stability of Al-Sn-Zn-In-O thin film transistors by adopting AlO_x passivation layer. Appl Phys Lett 2010;96(21):213511.
[32] Li F, Nathan A. CCD image sensors in deep-ultraviolet. Berlin/Heidelberg: Springer-Verlag; 2005.